AIP | The Journal of Chemical Physics

Rotational analysis and deperturbation of the A 2Π → X 2Σ+ and B′ 2Σ+ → X 2Σ+ emission spectra of MgH

Alireza Shayesteh and Peter F. Bernath

Citation: J. Chem. Phys. **135**, 094308 (2011); doi: 10.1063/1.3631341
View online: http://dx.doi.org/10.1063/1.3631341
View Table of Contents: http://jcp.aip.org/resource/1/JCPSA6/v135/i9
Published by the American Institute of Physics.

Rotational analysis and deperturbation of the $A\,^2\Pi \rightarrow X\,^2\Sigma^+$ and $B'\,^2\Sigma^+ \rightarrow X\,^2\Sigma^+$ emission spectra of MgH

Alireza Shayesteh[1,a)] and Peter F. Bernath[2,b)]
[1]*School of Chemistry, College of Science, University of Tehran, Tehran 14176, Iran*
[2]*Department of Chemistry, University of York, Heslington, York YO10 5DD, United Kingdom*

(Received 12 June 2011; accepted 8 August 2011; published online 6 September 2011)

Deperturbation analysis of the $A\,^2\Pi \rightarrow X\,^2\Sigma^+$ and $B'\,^2\Sigma^+ \rightarrow X\,^2\Sigma^+$ emission spectra of ^{24}MgH is reported. Spectroscopic data for the v = 0 to 3 levels of the $A\,^2\Pi$ state and the v = 0 to 4 levels of the $B'\,^2\Sigma^+$ state were fitted together using a single Hamiltonian matrix that includes $^2\Pi$ and $^2\Sigma^+$ matrix elements, as well as off-diagonal elements coupling several vibrational levels of the two states. A Dunham-type fit was performed and the resulting $Y_{l,0}$ and $Y_{l,1}$ coefficients were used to generate Rydberg–Klein–Rees (RKR) potential curves for the $A\,^2\Pi$ and the $B'\,^2\Sigma^+$ states. Vibrational overlap integrals were computed from the RKR potentials, and the off-diagonal matrix elements coupling the electronic wavefunctions (a^+ and b) were determined. Zero point dissociation energies (D_0) of the $A\,^2\Pi$ and $B'\,^2\Sigma^+$ states of ^{24}MgH were determined to be 12 957.5 ± 0.5 and 10 133.6 ± 0.5 cm^{-1}, respectively. Using the $Y_{0,1}$ coefficients, the equilibrium internuclear distances (r_e) of the $A\,^2\Pi$ and $B'\,^2\Sigma^+$ states were determined to be 1.67827(1) Å and 2.59404(4) Å, respectively.
 [doi:10.1063/1.3631341]

I. INTRODUCTION

Since 1907 when its first laboratory spectra[1,2] were recorded, MgH has been an important molecule in astrophysics. The $A\,^2\Pi \rightarrow X\,^2\Sigma^+$ visible bands of MgH appear strongly in the absorption spectra of the sun and of some cool stars,[3–5] and are used to estimate the magnesium isotope abundances.[6,7] In the first series of spectroscopic studies on MgH, in the 1920s and 1930s, several electronic transitions involving the $X\,^2\Sigma^+$ ground electronic state and the low-lying excited states were observed and analyzed.[8–17] Balfour and co-workers studied the visible and ultraviolet spectra of MgH and MgD extensively in the 1970s.[18–25] They produced MgH in a magnesium arc source, and recorded the $A\,^2\Pi \rightarrow X\,^2\Sigma^+$ and $B'\,^2\Sigma^+ \rightarrow X\,^2\Sigma^+$ emission spectra using a spectrograph. They also reported spectroscopic constants for the ground and excited electronic states, and observed several local perturbations in the $A\,^2\Pi$ and $B'\,^2\Sigma^+$ states.

The $A\,^2\Pi \rightarrow X\,^2\Sigma^+$ emission spectrum of MgH was recorded by Bernath *et al.* at very high resolution using a Fourier transform spectrometer,[26] and only the low-J lines were analyzed in order to predict the microwave and infrared spectra of MgH. The diode-laser-infrared and the microwave spectra of MgH were recorded and analyzed soon after Bernath's work.[27–31] High resolution Fourier transform infrared emission spectra of MgH and MgD were recorded in 2003, and a combined-isotopologue analysis of all the infrared and microwave data available in the literature was performed using a Dunham-type energy level expression.[32]

MgH has also been the subject of several theoretical studies since the 1970s, and its equilibrium internuclear distance, vibrational frequencies, dissociation energies, and dipole moments have been computed by various *ab initio* theoretical methods.[33–37] Because of the importance of MgH in astrophysics, the line and continuum opacities of MgH in cool stellar atmospheres were calculated by Kirby and co-workers,[38–41] using *ab initio* potential energy curves and transition dipole moments. Recently, Mestdagh *et al.*[42] and Guitou *et al.*[43] computed the potential energy curves for the ground and several excited states of MgH using high-level *ab initio* methods with large basis sets.

In a recent paper we reported new high-resolution emission spectra of the $A\,^2\Pi \rightarrow X\,^2\Sigma^+$ and $B'\,^2\Sigma^+ \rightarrow X\,^2\Sigma^+$ transitions of MgH.[44] The electronic data, combined with all

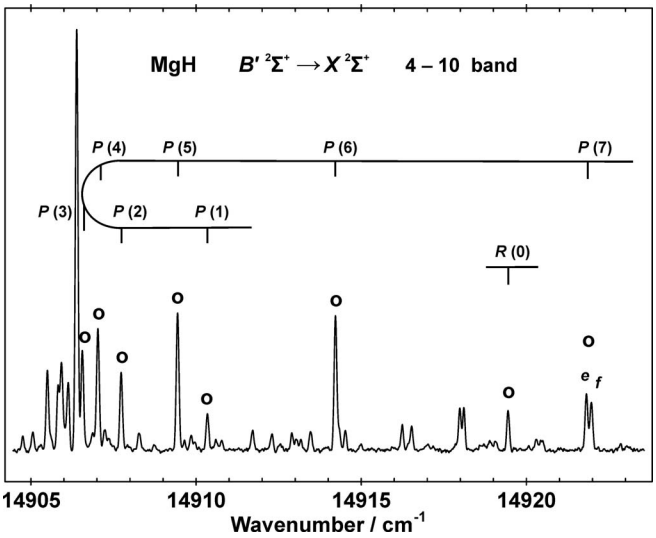

FIG. 1. A portion of the $B'\,^2\Sigma^+ \rightarrow X\,^2\Sigma^+$ emission spectrum of MgH showing lines from the 4–10 band (marked with circles). A small perturbation is seen in the $P(7)$ line, i.e., $N' = 6$, which is caused by the v = 4 level of the $A\,^2\Pi$ state.

a)Electronic mail: ashayesteh@ut.ac.ir.
b)Electronic mail: peter.bernath@york.ac.uk.

TABLE I. The highest N values observed for the vibrational levels of the $A\,^2\Pi$ and $B'\,^2\Sigma^+$ states.[a]

$A\,^2\Pi$ state		$B'\,^2\Sigma^+$ state	
v	highest N	v	highest N
0	42	0	49
1	36	1	48
2	30	2	40[b]
3	24[c]	3	33[d]
		4	20

[a]$\mathbf{N} = \mathbf{R} + \mathbf{L} = \mathbf{J} - \mathbf{S}$
[b]Data in Ref. 24 extend up to $N = 22$.
[c]Data in Ref. 23 extend up to $N = 15$, and some low-N lines in the $v' = 3$ bands were assigned incorrectly.
[d]Data in Ref. 24 extend up to $N = 24$.

the infrared and microwave data available in the literature, spanned the v = 0 to 11 levels of the $X\,^2\Sigma^+$ ground state, and the v = 0 to 3 levels of the $A\,^2\Pi$ and the $B'\,^2\Sigma^+$ excited states. A direct-potential-fit was performed for the $X\,^2\Sigma^+$ ground state, while all the rotational levels of the $A\,^2\Pi$ and $B'\,^2\Sigma^+$ excited states were fitted as individual term values. The $v'' = 11$ level was found to be the highest bound vibrational level of the $X\,^2\Sigma^+$ ground state, and the zero-point dissociation energy of MgH was determined to be $D_0 = 10\,365.6 \pm 0.5$ cm^{-1} (1.28517 ± 0.00006 eV).[44] Rotational analysis and deperturbation of the observed vibrational levels of the $A\,^2\Pi$ and $B'\,^2\Sigma^+$ electronic states is reported here.

II. EXPERIMENT AND RESULTS

The experimental conditions have been described in our previous paper.[44] The MgH radical was generated in a discharge-furnace source, and the emission spectra were recorded using a Bruker IFS 120 HR Fourier transform spectrometer.[44] The $B'\,^2\Sigma^+ \rightarrow X\,^2\Sigma^+$ spectrum (9000 −18 000 cm^{-1}) was recorded at 650 °C with an instrumental resolution of 0.0375 cm^{-1}, and the $A\,^2\Pi \rightarrow X\,^2\Sigma^+$ spectrum (16 000−23 000 cm^{-1}) was recorded at 550 °C with an instrumental resolution of 0.065 cm^{-1}. Hundreds of scans were coadded, resulting in a signal-to-noise ratio of about 1000 for the strongest emission lines of MgH. The spectra were calibrated to an absolute accuracy of better than 0.005 cm^{-1}, as described in our previous paper.[44] In addition to the bands analyzed in Ref. 44, we assigned three more bands for the $B'\,^2\Sigma^+ \rightarrow X\,^2\Sigma^+$ system, i.e, the 4 → 2, 4 → 10, and 4 → 11 bands. An expanded view of the 4 → 10 band is displayed in Fig. 1. Overall, the data spanned the $v'' = 0$ to 11 of the $X\,^2\Sigma^+$ ground state, the $v' = 0$ to 3 of the $A\,^2\Pi$ state and the $v' = 0$

TABLE II. Matrix elements of the $\mathbf{N^2}$ Hamiltonian; F_1 and F_2 correspond to $^2\Pi_{1/2}$ and $^2\Pi_{3/2}$ basis functions, respectively, and the upper and lower signs refer to e and f parities, respectively.[a]

Constant		Matrix elements	Constant		Matrix elements
B	1,1	$z + 2$	L	1,1	$(z^2 + 12z + 16)(z + 1)^2$
	2,2	z		2,2	$z(z + 4)(z + 1)^2$
	1,2	$-\sqrt{z}$		1,2	$-4(z + 2)(z + 1)^2\sqrt{z}$
D	1,1	$-(z + 4)(z + 1)$	M	1,1	$(z + 2)(z^2 + 16z + 16)(z + 1)^2$
	2,2	$-z(z + 1)$		2,2	$z(z^2 + 8z + 8)(z + 1)^2$
	1,2	$2(z + 1)\sqrt{z}$		1,2	$-(5z^2 + 20z + 16)(z + 1)^2\sqrt{z}$
H	1,1	$(z^2 + 8z + 8)(z + 1)$	N	1,1	$(z^3 + 24z^2 + 80z + 64)(z + 1)^3$
	2,2	$z(z + 2)(z + 1)$		2,2	$z(z^2 + 12z + 16)(z + 1)^3$
	1,2	$-(3z + 4)(z + 1)\sqrt{z}$		1,2	$-2(3z + 4)(z + 4)(z + 1)^3\sqrt{z}$
A	1,1	-0.5	p	1,1	$\mp 0.5(J + 0.5)$
	2,2	$+0.5$		2,2	0
	1,2	0		1,2	0
A_D	1,1	$-0.5(z + 2)$	p_D	1,1	$\mp 0.5(J + 0.5)(z + 2)$
	2,2	$+0.5z$		1,2	$\pm 0.25(J + 0.5)\sqrt{z}$
A_H	1,1	$-0.5(z + 4)(z + 1)$	p_H	1,1	$\mp 0.5(J + 0.5)(z + 4)(z + 1)$
	2,2	$+0.5z(z + 1)$		1,2	$\pm 0.5(J + 0.5)(z + 1)\sqrt{z}$
A_L	1,1	$-0.5(z^2 + 8z + 8)(z + 1)$	p_L	1,1	$\mp 0.5(J + 0.5)(z^2 + 8z + 8)(z + 1)$
	2,2	$+0.5z(z + 2)(z + 1)$		1,2	$\pm 0.25(J + 0.5)(3z + 4)(z + 1)\sqrt{z}$
γ	1,1	–1	q	1,1	$\mp(J + 0.5)$
	2,2	0		2,2	0
	1,2	$0.5\sqrt{z}$		1,2	$\pm 0.5(J + 0.5)\sqrt{z}$
γ_D	1,1	$-0.5(3z + 4)$	q_D	1,1	$\mp 0.5(J + 0.5)(3z + 4)$
	2,2	$-0.5z$		2,2	$\mp 0.5(J + 0.5)z$
	1,2	$0.5(z + 2)\sqrt{z}$		1,2	$\pm 0.5(J + 0.5)(z + 2)\sqrt{z}$
γ_H	1,1	$-2(z + 2)(z + 1)$	q_H	1,1	$\mp 2(J + 0.5)(z + 2)(z + 1)$
	2,2	$-z(z + 1)$		2,2	$\mp(J + 0.5)z(z + 1)$
	1,2	$0.5(z + 4)(z + 1)\sqrt{z}$		1,2	$\pm 0.5(J + 0.5)(z + 4)(z + 1)\sqrt{z}$
γ_L	1,1	$-0.5(5z^2 + 20z + 16)(z + 1)$	q_L	1,1	$\mp 0.5(J + 0.5)(5z^2 + 20z + 16)(z + 1)$
	2,2	$-0.5z(3z + 4)(z + 1)$		2,2	$\mp 0.5(J + 0.5)z(3z + 4)(z + 1)$
	1,2	$0.5(z^2 + 8z + 8)(z + 1)\sqrt{z}$		1,2	$\pm 0.5(J + 0.5)(z^2 + 8z + 8)(z + 1)\sqrt{z}$

[a]$z = J(J + 1) - 3/4 = (J + 1/2)^2 - 1 = (J - 1/2)(J + 3/2)$.

to 4 of the $B'\ ^2\Sigma^+$ state. Compared to Balfour's data obtained in 1970s, the new data have much higher precision and accuracy, and extend to higher rotational quantum numbers (Table I).

III. DATA ANALYSIS

In our previous work on MgH,[44] the $A\ ^2\Pi \rightarrow X\ ^2\Sigma^+$ and $B'\ ^2\Sigma^+ \rightarrow X\ ^2\Sigma^+$ data, combined with all available infrared and microwave data from Ref. 32, were analyzed using a direct-potential-fit for the $X\ ^2\Sigma^+$ ground state, while the rovibronic energy levels of the $A\ ^2\Pi$ and $B'\ ^2\Sigma^+$ states were fitted as individual term values. This analysis resulted in an analytic radial potential energy function for the $X\ ^2\Sigma^+$ ground state,[44] and the dissociation energy of the $X\ ^2\Sigma^+$ state was determined accurately. In that article, we also reported term values for $v' = 0$ to 3 of the $A\ ^2\Pi$ and $B'\ ^2\Sigma^+$ states with a typical accuracy of 0.005 cm^{-1}. The newly assigned bands involving the $v' = 4$ of the $B'\ ^2\Sigma^+$ state have been added and the term values for the $v' = 4$ vibrational level have been determined by setting the ground state potential energy function fixed to the one reported in Ref. 44. Complete lists of transition wavenumbers and term values (relative to the $v'' = 0$, $N'' = 0$, $J'' = 0.5$ level of the $X\ ^2\Sigma^+$ ground state) are presented in the supplementary material.[45] For rotational analysis and deperturbation of the $A\ ^2\Pi$ and $B'\ ^2\Sigma^+$ excited states, we used the term values listed in Table S3 of the supplementary material[45] as input for our least-squares fitting program.

A. Hamiltonian matrices

The rotational energy levels of the $A\ ^2\Pi$ state of MgH follow a pattern which is an intermediate between Hund's cases (a) and (b), whereas the $B'\ ^2\Sigma^+$ state is a pure Hund's case (b) state. The $\mathbf{N^2}$ effective Hamiltonian of Brown[46] was used for the unperturbed energy levels of the $A\ ^2\Pi$ and $B'\ ^2\Sigma^+$ states. Matrix elements of the effective Hamiltonian for the $A\ ^2\Pi$ state (2×2) were derived using the Hund's case (a) basis functions and are listed in Table II. Although we used the Hund's case (a) basis functions, the eigenvalues of the Hamiltonian matrix, i.e., the actual level energies, are independent of the choice of basis functions. For the $B'\ ^2\Sigma^+$ state, the following energy expressions in which $x = N(N+1)$ were used for the e and f parity sublevels:

$$E\,(^2\Sigma^+) = B\,x - D\,x^2 + H\,x^3 + L\,x^4 + M\,x^5 + \Delta E_{\mathrm{Spin-Rot}}, \tag{1a}$$

$$\Delta E^{e}_{\mathrm{Spin-Rot}} = +\frac{1}{2}\,(\gamma + \gamma_D\,x + \gamma_H\,x^2)\,(N), \tag{1b}$$

$$\Delta E^{f}_{\mathrm{Spin-Rot}} = -\frac{1}{2}\,(\gamma + \gamma_D\,x + \gamma_H\,x^2)\,(N+1). \tag{1c}$$

The B_v values of the $A\ ^2\Pi$ state vibrational levels are significantly larger than those of the $B'\ ^2\Sigma^+$ state levels, and several level crossings occur between these states. An illustration of these level crossings is presented in Fig. 2, in which the observed term values of the F_{1e} components[47] of the $A\ ^2\Pi$ and $B'\ ^2\Sigma^+$ states are plotted versus $N(N+1)$. The general selection rules for local perturbations occurring between the $A\ ^2\Pi$ and $B'\ ^2\Sigma^+$ states are: $\Delta J = 0$, $+ \leftrightarrow +$ or $- \leftrightarrow -$ (total parity), and $e \leftrightarrow e$ or $f \leftrightarrow f$ (rotationless parity). The $A\ ^2\Pi$ state resembles Hund's case (b) at high J's, and therefore, perturbations for which $\Delta N \neq 0$ are expected to be relatively weak. In the absence of local perturbations between the $A\ ^2\Pi$ and $B'\ ^2\Sigma^+$ states, the Hamiltonian matrices described above should reproduce all the observed level energies. In order to take the local perturbations into account, the following off-diagonal matrix elements in which the upper (lower) sign refers to e (f) parity should be added to the Hamiltonian:[48]

$$\left\langle {}^2\Pi_{1/2}\middle|\hat{\mathbf{H}}_{\mathrm{Rot}} + \hat{\mathbf{H}}_{\mathrm{SO}}\middle|{}^2\Sigma^+_{1/2}\right\rangle = \frac{a_{v_\Pi, v_\Sigma}}{2} + bB_{v_\Pi, v_\Sigma} \times \left[1 \mp \left(J + \frac{1}{2}\right)\right], \tag{2}$$

$$\left\langle {}^2\Pi_{3/2}\middle|\hat{\mathbf{H}}_{\mathrm{Rot}} + \hat{\mathbf{H}}_{\mathrm{SO}}\middle|{}^2\Sigma^+_{1/2}\right\rangle = -bB_{v_\Pi, v_\Sigma}\sqrt{\left(J - \frac{1}{2}\right)\left(J + \frac{3}{2}\right)}. \tag{3}$$

The parameters a_{v_Π, v_Σ} and B_{v_Π, v_Σ} in Eqs. (2) and (3) are defined as[48]

$$a_{v_\Pi, v_\Sigma} = a^+ \langle v_\Pi \mid v_\Sigma \rangle, \tag{4}$$

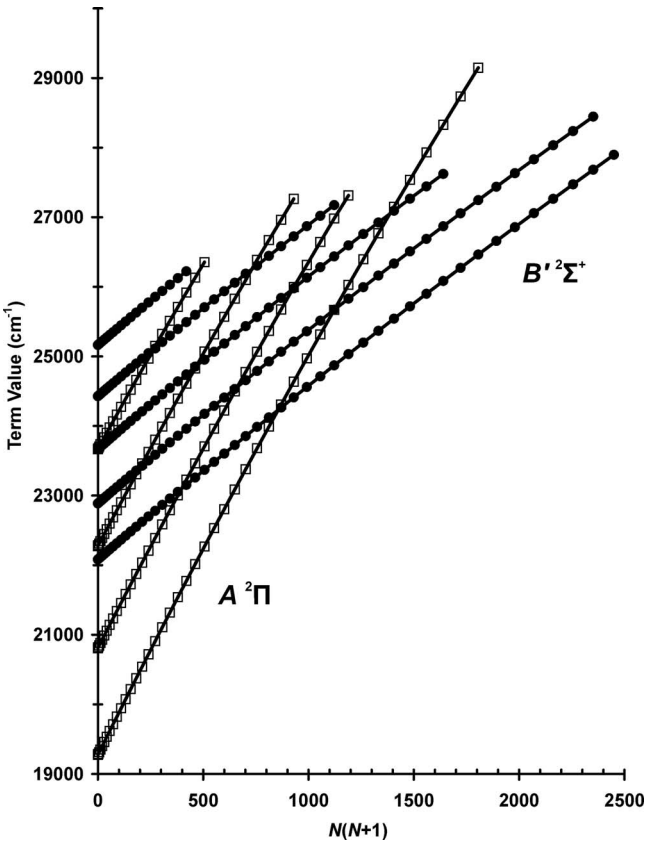

FIG. 2. A plot of term values of the F_{1e} components of the $A\ ^2\Pi$ and $B'\ ^2\Sigma^+$ states versus $N(N+1)$, displaying the N values at which vibrational levels cross. Term values for v = 0, 1, 2, and 3 of the $A\ ^2\Pi$ state are marked with squares and those for v = 0, 1, 2, 3, and 4 of the $B'\ ^2\Sigma^+$ state are marked with full circles.

$$B_{v_\Pi,v_\Sigma} = \frac{\hbar^2}{2\mu} \langle v_\Pi | \frac{1}{r^2} | v_\Sigma \rangle , \quad (5)$$

while the purely electronic constants a^+ and b are the following:[48,49]

$$a^+ = \langle \pi | a l^+ | \sigma \rangle , \quad (6)$$

$$b = \langle \pi | l^+ | \sigma \rangle . \quad (7)$$

The constants a_{v_Π,v_Σ} and bB_{v_Π,v_Σ} were determined for each pair of interacting vibrational levels (v_Π , v_Σ) from least-squares fitting of all the term values. A single Hamiltonian matrix (15 × 15) was generated for the v = 0, 1, 2, 3, and 4 vibrational levels of the $A\ ^2\Pi$ and $B'\ ^2\Sigma^+$ states; the unobserved v = 4 level of the $A\ ^2\Pi$ state was included in the matrix because of its interaction with the v = 4 of $B'\ ^2\Sigma^+$ state (Fig. 1). Each vibrational level of the $A\ ^2\Pi$ state required a 2 × 2 block of the matrix due to the existence of $^2\Pi_{1/2}$ and $^2\Pi_{3/2}$ components,[47] while the energy expression in Eq. (1) was used for each vibrational level of the $B'\ ^2\Sigma^+$ state. Several off-diagonal matrix elements, connecting the vibrational levels of the $A\ ^2\Pi$ and $B'\ ^2\Sigma^+$ states, were also included (as in Eqs. (2) and (3)). Instead of the usual "band constants," we used the following Dunham-type expressions for the A_v, γ_v, p_v, and q_v constants:

$$A_v = A_e + \sum_{k=1} A_k \left(v + \frac{1}{2}\right)^k , \quad (8)$$

$$\gamma_v = \gamma_e + \sum_{k=1} \gamma_k \left(v + \frac{1}{2}\right)^k . \quad (9)$$

TABLE III. Dunham-type constants for the $A\ ^2\Pi$ and $B'\ ^2\Sigma^+$ states (in cm^{-1}), and the off-diagonal parameters coupling various vibrational levels of the two states. Energies are relative to the $v'' = 0$, $N'' = 0$ level of the $X\ ^2\Sigma^+$ ground state, and the numbers in parentheses are 1σ uncertainties in the last quoted digits.

$A\ ^2\Pi$ state		Off-diagonal		$B'\ ^2\Sigma^+$ state	
U_e	18486.4242(39)		a_{v_Π,v_Σ} (cm^{-1})	U_e	21671.0091(77)
$Y_{1,0}$	1600.3344(88)	$a_{0,1}$	0.2188(87)	$Y_{1,0}$	828.6003(216)
$Y_{2,0}$	–31.8697(51)	$a_{0,2}$	0.436(61)	$Y_{2,0}$	–11.8368(175)
$Y_{3,0}$	–0.52724(84)	$a_{0,3}$	0.938(42)	$Y_{3,0}$	0.05761(528)
$Y_{0,1}$	6.188157(40)	$a_{0,4}$	1.68(39)	$Y_{4,0}$	–0.00382(53)
$Y_{1,1}$	–0.185546(86)	$a_{1,0}$	–0.24(17)	$Y_{0,1}$	2.590193(40)
$Y_{2,1}$	–0.001900(46)	$a_{1,1}$	–0.774(36)	$Y_{1,1}$	0.014179(88)
$Y_{3,1}$	–0.0003421(71)	$a_{1,2}$	–1.6165(86)	$Y_{2,1}$	–0.003080(64)
$10^4\ Y_{0,2}$	–3.69903(101)	$a_{1,3}$	–2.696(14)	$Y_{3,1}$	–0.0001506(179)
$10^4\ Y_{1,2}$	–0.01835(198)	$a_{1,4}$	–4.26(32)	$Y_{4,1}$	0.0000162(17)
$10^4\ Y_{2,2}$	–0.00202(87)	$a_{2,1}$	1.884(21)	$10^4\ Y_{0,2}$	–1.012145(692)
$10^4\ Y_{3,2}$	–0.00190(11)	$a_{2,2}$	3.4123(71)	$10^4\ Y_{1,2}$	–0.13491(81)
$10^8\ Y_{0,3}$	1.56315(848)	$a_{2,3}$	4.8267(95)	$10^4\ Y_{2,2}$	0.00069(33)
$10^8\ Y_{1,3}$	–0.060(14)	$a_{2,4}$	5.877(49)	$10^4\ Y_{3,2}$	0.000144(43)
$10^8\ Y_{2,3}$	–0.0399(29)	$a_{3,2}$	–5.4342(61)	$10^8\ Y_{0,3}$	0.8841(63)
$10^{12}\ Y_{0,4}$	–1.370(25)	$a_{3,3}$	–6.1528(63)	$10^8\ Y_{1,3}$	0.1145(36)
$10^{12}\ Y_{1,4}$	–0.393(35)	$a_{3,4}$	–5.224(25)	$10^8\ Y_{2,3}$	0.00382(64)
A_e	34.9871(75)	$a_{4,4}$	1.639(89)	$10^{12}\ Y_{0,4}$	–1.208(28)
A_1	0.0484(88)			$10^{12}\ Y_{1,4}$	–0.0851((57)
A_2	–0.0134(21)			$10^{16}\ Y_{0,5}$	0.904(46)
$10^2\ \gamma_e$	–1.458(26)		bB_{v_Π,v_Σ} (cm^{-1})	$10^2\ \gamma_e$	1.514(37)
$10^2\ \gamma_1$	0.203(22)	$bB_{0,1}$	0.029267(65)	$10^2\ \gamma_1$	1.159(61)
$10^2\ \gamma_2$	–0.0478(50)	$bB_{0,2}$	0.06658(44)	$10^2\ \gamma_2$	–0.413(27)
$10^6\ \gamma_{D,e}$	2.98(50)	$bB_{0,3}$	0.12673(30)	$10^2\ \gamma_3$	0.0410(37)
$10^6\ \gamma_{D,1}$	2.08(17)	$bB_{0,4}$	0.2603(35)	$10^6\ \gamma_{D,e}$	1.83(47)
$10^{10}\ \gamma_{H,e}$	9.9(26)	$bB_{1,0}$	–0.0336(22)	$10^6\ \gamma_{D,1}$	–7.22(51)
$10^2\ p_e$	2.773(45)	$bB_{1,1}$	–0.10405(36)	$10^6\ \gamma_{D,2}$	0.983(96)
$10^2\ p_1$	–0.420(41)	$bB_{1,2}$	–0.215969(72)	$10^{10}\ \gamma_{H,e}$	–6.8(16)
$10^2\ p_2$	0.1091(92)	$bB_{1,3}$	–0.35802(13)	$10^{10}\ \gamma_{H,1}$	16.1(13)
$10^6\ p_{D,e}$	–5.85(86)	$bB_{1,4}$	–0.4294(67)		
$10^6\ p_{D,1}$	–3.75(29)	$bB_{2,1}$	0.24998(40)		
$10^{10}\ p_{H,e}$	–17.0(45)	$bB_{2,2}$	0.456701(94)		
$10^2\ q_e$	0.2040(16)	$bB_{2,3}$	0.645500(92)		
$10^2\ q_1$	–0.0582(18)	$bB_{2,4}$	0.76705(84)		
$10^2\ q_2$	0.01581(35)	$bB_{3,2}$	–0.7286(13)		
$10^6\ q_{D,e}$	–0.760(31)	$bB_{3,3}$	–0.82354(12)		
$10^6\ q_{D,1}$	–0.032(30)	$bB_{3,4}$	–0.70763(39)		
$10^{10}\ q_{H,e}$	0.44(20)	$bB_{4,4}$	0.2515(30)		
$10^{10}\ q_{H,1}$	–5.18(26)				

TABLE IV. Empirical band constants for the $A\,^2\Pi$ and $B'\,^2\Sigma^+$ states (in cm^{-1}), relative to the $v'' = 0$, $N'' = 0$ level of the $X\,^2\Sigma^+$ ground state. These constants should be combined with the off-diagonal parameters of Table III to reproduce the term values. 1σ uncertainties are quoted in parentheses.

	$A\,^2\Pi$ state				
	v = 0	v = 1	v = 2	v = 3	v = 4 (fixed)[a]
T_v	19 278.5575(10)	20 813.4399(11)	22 279.8354(12)	23 674.5875(13)	24 994.523
A_v	35.0072(37)	35.0294(37)	35.0250(35)	34.9857(40)	34.934
B_v	6.094878(11)	5.904407(16)	5.707126(24)	5.500717(24)	5.28355
$10^4\,D_v$	3.70939(30)	3.73765(57)	3.7905(12)	3.8606(11)	3.996
$10^8\,H_v$	1.5283(29)	1.3879(72)	1.228(22)	0.586(13)	0.485
$10^{12}\,L_v$	–1.5856(61)	–1.993(30)	–2.74(13)	…	–3.14
$10^2\,\gamma_v$	–1.378(16)	–1.244(20)	–1.250(14)	–1.404(22)	–1.51
$10^6\,\gamma_{D,v}$	4.24(37)	5.36(60)	8.92(21)	12.44(55)	12.3
$10^{10}\,\gamma_{H,v}$	8.8(20)	16.0(43)	…	…	9.9
$10^2\,p_v$	2.618(28)	2.360(34)	2.427(24)	2.678(35)	3.09
$10^6\,p_{D,v}$	–8.66(67)	–9.9(11)	–17.10(38)	–20.29(96)	–22.7
$10^{10}\,p_{H,v}$	–11.4(37)	–29.7(79)	…	…	–17.
$10^2\,q_v$	0.17927(81)	0.1473(12)	0.1504(17)	0.2206(15)	0.262
$10^6\,q_{D,v}$	–0.782(16)	–0.642(34)	–0.645(61)	–2.278(38)	–0.90
$10^{10}\,q_{H,v}$	–2.143(79)	–8.47(23)	–13.91(51)	…	–22.9
	$B'\,^2\Sigma^+$ state				
	v = 0	v = 1	v = 2	v = 3	v = 4
T_v	22 082.3562(13)	22 887.4550(14)	23 669.2761(15)	24 428.0112(14)	25 163.6838(46)
B_v	2.596509(16)	2.604053(17)	2.604715(16)	2.597954(21)	2.584910(87)
$10^4\,D_v$	1.07983(49)	1.21095(54)	1.34298(46)	1.46524(75)	1.6036(39)
$10^8\,H_v$	0.9468(58)	1.0480(66)	1.1720(45)	1.2624(94)	1.470(51)
$10^{12}\,L_v$	–1.270(29)	–1.261(34)	–1.144(14)	–1.070(38)	…
$10^{16}\,M_v$	0.934(51)	0.784(63)	…	…	…
$10^2\,\gamma_v$	2.002(15)	2.481(16)	2.370(20)	2.483(26)	1.665(37)
$10^6\,\gamma_{D,v}$	–1.76(25)	–6.71(27)	–8.68(46)	–17.53(91)	…
$10^{10}\,\gamma_{H,v}$	2.32(95)	16.5(11)	29.0(24)	92.1(72)	…

[a]Band constants for the unobserved v = 4 level of the $A\,^2\Pi$ state were calculated from the Dunham-type constants of Table III and held fixed.

$$p_v = p_e + \sum_{k=1} p_k \left(v + \frac{1}{2}\right)^k, \tag{10}$$

$$q_v = q_e + \sum_{k=1} q_k \left(v + \frac{1}{2}\right)^k. \tag{11}$$

Similar Dunham-type expressions were used for the higher-order parameters $\gamma_{D,v}$, $p_{D,v}$, $q_{D,v}$, etc. The vibronic energy (T_v), inertial rotational constant (B_v), and the centrifugal distortion constants (D_v, H_v, L_v, and M_v) were represented by the well-known Dunham coefficients ($Y_{l,m}$).

B. Least-squares fitting

The observed level energies of the $A\,^2\Pi$ and $B'\,^2\Sigma^+$ states (term values of Table S3 in the supplementary material)[45] were fitted using the 15 × 15 Hamiltonian matrix described above, and resulted in the determination of unperturbed Dunham parameters for the $A\,^2\Pi$ and $B'\,^2\Sigma^+$ states as well as the perturbation matrix elements a_{v_Π,v_Σ} and bB_{v_Π,v_Σ} (Table III). Although the v = 4 level of the $A\,^2\Pi$ state was not observed in our spectra, it is obvious from the Dunham-type fit that this level is responsible for the low-N perturbations observed in the v = 4 level of the $B'\,^2\Sigma^+$ state (Fig. 1), and we were able to determine the $a_{4,4}$ and $bB_{4,4}$ constants.

The Dunham-type fit has an overall dimensionless standard error (DSE) of 1.15, which means that the 102 parameters listed in Table III can reproduce the data (905 term values) typically to within $\pm 0.006\ cm^{-1}$. We performed another fit in which all the parameters of the $A\,^2\Pi$ and $B'\,^2\Sigma^+$ states were fitted as band constants, while those of the unobserved v = 4 level of the $A\,^2\Pi$ state were held fixed. The off-diagonal matrix elements a_{v_Π,v_Σ} and bB_{v_Π,v_Σ} were also fixed to the values listed in Table III. This band constant fit employed a total of 142 parameters, of which 49 were held fixed, and a DSE of 0.97 was obtained. The band constants are listed in Table IV. We also tried an even more flexible fit in which the band constants and the off-diagonal matrix elements a_{v_Π,v_Σ} and bB_{v_Π,v_Σ} were all varied freely (142 parameters, of which 15 were held fixed). Although this fit resulted in a DSE of 0.87, several parameters

TABLE V. The values of rotational quantum number N at which the levels cross; ($\mathbf{N} = \mathbf{R} + \mathbf{L} = \mathbf{J} - \mathbf{S}$).

	$v_\Sigma = 0$	$v_\Sigma = 1$	$v_\Sigma = 2$	$v_\Sigma = 3$	$v_\Sigma = 4$
$v_\Pi = 0$	29	33	37	40	43
$v_\Pi = 1$	19	25	30	34	37
$v_\Pi = 2$		14	21	27	31
$v_\Pi = 3$			3	16	23
$v_\Pi = 4$					7

TABLE VI. The Dunham coefficients (in cm^{-1}) used for generation of RKR potentials, and the turning points for the observed vibrational levels.[a,b]

	$A\ ^2\Pi$ state	r_e (Å)	1.67827(1)	v	r_{min} (Å)	r_{max} (Å)
U_e	18 486.4242	$Y_{0,1}$	6.188157	0	1.5445	1.8422
$Y_{1,0}$	1600.3344	$Y_{1,1}$	–0.185546	1	1.4621	1.9870
$Y_{2,0}$	–31.8697	$Y_{2,1}$	–0.001900	2	1.4121	2.1031
$Y_{3,0}$	–0.52724	$Y_{3,1}$	–0.0003421	3	1.3753	2.2104
	$B'\ ^2\Sigma^+$ state	r_e (Å)	2.59404(4)	v	r_{min} (Å)	r_{max} (Å)
U_e	21 671.0801	$Y_{0,1}$	2.5905698	0	2.3937	2.8064
$Y_{1,0}$	828.3237	$Y_{1,1}$	0.0128228	1	2.2523	2.9758
$Y_{2,0}$	–11.4774	$Y_{2,1}$	-1.510×10^{-3}	2	2.1578	3.1034
$Y_{3,0}$	–0.160	$Y_{3,1}$	-9.5693×10^{-4}	3	2.0834	3.2162
$Y_{4,0}$	0.0636	$Y_{4,1}$	2.151×10^{-4}	4	2.0210	3.3222
$Y_{5,0}$	–0.01069	$Y_{5,1}$	-2.2302×10^{-5}	5	1.967	3.425
$Y_{6,0}$	8.1038×10^{-4}	$Y_{6,1}$	8.50×10^{-7}	6	1.920	3.527
$Y_{7,0}$	-2.50×10^{-5}			7	1.878	3.630
				8	1.840	3.736
				9	1.806	3.845

[a]For the $B'\ ^2\Sigma^+$ state, data for the $v' = 5$ to 9 levels from Ref. 24 were included, and higher order $Y_{l,0}$ and $Y_{l,1}$ constants were determined in order to obtain a more accurate RKR potential (see text).

[b]The equilibrium internuclear distances (r_e) were calculated from $Y_{0,1}$ constants of Table III and were reported with 2σ uncertainties.

in the fit were highly correlated and some of them may not be physically significant; the constants of this fit are listed in the supplementary material.[45] Our "recommended" set of constants for the $A\ ^2\Pi$ and $B'\ ^2\Sigma^+$ states of ^{24}MgH are those listed in Table III, i.e., 68 Dunham-type and 34 off-diagonal a_{v_Π,v_Σ} and bB_{v_Π,v_Σ} parameters. On the other hand, when the empirical band constants of Table IV are combined with the off-diagonal a_{v_Π,v_Σ} and bB_{v_Π,v_Σ} parameters of Table III, they can reproduce the term values more accurately.

From the band constants of Table IV, the "unperturbed" level energies of the $A\ ^2\Pi$ and $B'\ ^2\Sigma^+$ states were calculated, while all a_{v_Π,v_Σ} and bB_{v_Π,v_Σ} constants were set to zero. These level energies were subtracted from the observed (perturbed) term values listed in Table S3, and the term value shifts were calculated. For example, for the strong perturbation between the $v_\Pi = 3$ and $v_\Sigma = 3$ levels at $N = 16$, term value shifts of about ± 13.0 cm^{-1} were found. A complete list of term value shifts is provided in the supplementary material.[45] For each pair of interacting vibrational levels, the N value at which level crossing occurs was found (see Table V).

C. Rydberg–Klein–Rees (RKR) potential curves

For the $A\ ^2\Pi$ state, the Dunham coefficients $Y_{l,0}$ and $Y_{l,1}$ listed in Table III were imported in Le Roy's RKR1 program,[50] and the RKR potential curve (turning points) was obtained. For the $B'\ ^2\Sigma^+$ state potential curve, we first used the old $B'\ ^2\Sigma^+ \leftrightarrow X\ ^2\Sigma^+$ data reported by Balfour and Lindgren[24] to obtain moderately accurate term values for the $v' = 5$ to 9 vibrational levels of the $B'\ ^2\Sigma^+$ state. No *e/f* splitting was observed in the old data, and the term values for $v' = 5$ to 9 have a typical accuracy of about 0.1 cm^{-1}. These term values were added to our "unperturbed" term values for the $v' = 0$ to 4 levels and a new set of $Y_{l,0}$ and $Y_{l,1}$ coefficients, suitable for the entire $v' = 0$ to 9 vibrational range, were generated using Le Roy's DPARFIT program.[51] The RKR potential curve for the $B'\ ^2\Sigma^+$ state was obtained using the more extensive set of $Y_{l,0}$ and $Y_{l,1}$ coefficients presented in Table VI. The RKR turning points for all the observed vibrational levels are listed in Table VI, and the potential curves are plotted in Fig. 3.

TABLE VII. The vibrational integrals calculated from program LEVEL are compared with the observed a_{v_Π,v_Σ} and bB_{v_Π,v_Σ} parameters of Table III. The purely electronic matrix elements a^+ and b are calculated for each (v_Π, v_Σ) pair and averaged (see text).[a]

v_Π	v_Σ	N	$\langle v_\Pi \mid v_\Sigma \rangle$	a_{v_Π,v_Σ}(obs.) [cm^{-1}]	a^+ [cm^{-1}]	B_{v_Π,v_Σ} [cm^{-1}]	bB_{v_Π,v_Σ} (obs.) [cm^{-1}]	b
0	0	29	0.00341	...	...	0.012396	...	...
0	1	33	0.01147	0.2188(87)	19.07(76)	0.041808	0.029267(65)	0.7000(16)
0	2	37	0.02694	0.436(61)	16.2(23)[a]	0.097942	0.06658(44)	0.6798(45)[a]
0	3	40	0.04947	0.938(42)	18.96(85)	0.18036	0.12673(30)	0.7027(17)
0	4	43	0.07815	1.68(39)	21.5(50)[a]	0.28477	0.2603(35)	0.914(12)[a]
1	0	19	–0.01312	–0.24(17)	18(13)[a]	–0.047891	–0.0336(22)	0.702(45)[a]
1	1	25	–0.04045	–0.774(36)	19.14(88)	–0.14759	–0.10405(36)	0.7050(24)
1	2	30	–0.08513	–1.6165(86)	18.99(10)	–0.31003	–0.215969(72)	0.69660(23)
1	3	34	–0.1407	–2.696(14)	19.16(10)	–0.51254	–0.35802(13)	0.69852(25)
1	4	37	–0.1943	–4.26(32)	21.9(17)[a]	–0.71122	–0.4294(67)	0.6037(94)[a]
2	1	14	0.09873	1.884(21)	19.08(22)	0.35907	0.24998(40)	0.6962(11)
2	2	21	0.1801	3.4123(71)	18.944(39)	0.65615	0.456701(94)	0.69603(14)
2	3	27	0.2567	4.8267(95)	18.804(37)	0.93181	0.645500(92)	0.69274(10)
2	4	31	0.2975	5.877(49)	19.75(16)	1.0833	0.76705(84)	0.70807(78)
3	2	3	–0.2877	–5.4342(61)	18.886(21)	–1.0455	–0.7286(13)	0.6969(13)
3	3	16	–0.3278	–6.1528(63)	18.772(19)	–1.1917	–0.82354(12)	0.69108(10)
3	4	23	–0.2821	–5.224(25)	18.516(90)	–1.0239	–0.70763(39)	0.69113(38)
4	4	7	0.1057	1.639(89)	15.51(84)[a]	0.38342	0.2515(30)	0.6559(78)[a]
				Average:	19.0 ± 0.3		Average:	0.698 ± 0.005

[a] The numbers marked with asterisks were not used in averaging.

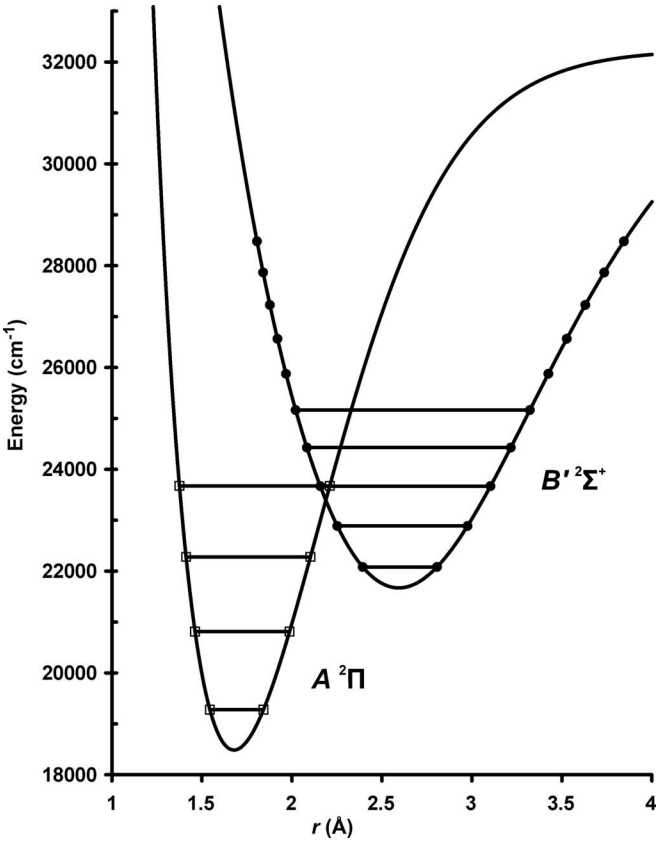

FIG. 3. Potential energy curves of the $A\,^2\Pi$ and $B'\,^2\Sigma^+$ states of MgH generated by program LEVEL using RKR turning points. The r_{min} and r_{max} turning points for the v = 0 to 3 levels of $A\,^2\Pi$ and the v = 0 to 9 levels of $B'\,^2\Sigma^+$ are displayed by squares and full circles, respectively.

D. Dissociation energies of $A\,^2\Pi$ and $B'\,^2\Sigma^+$ states

Dissociation energies were calculated for the $A\,^2\Pi$ and $B'\,^2\Sigma^+$ states using the dissociation energy of the $X\,^2\Sigma^+$ ground state ($D_0 = 10\,365.6 \pm 0.5$ cm^{-1}) and the energy levels of atomic magnesium. The $A\,^2\Pi$ and $B'\,^2\Sigma^+$ states both dissociate into Mg [3*s* 3*p*] (^{3}P) + H [1*s*] (^{2}S), whereas the $X\,^2\Sigma^+$ ground state dissociates into ground state atoms Mg [3s^2] (^{1}S) + H [1*s*] (^{2}S). The ^{3}P state of magnesium has $^3P_0$, $^3P_1$, and $^3P_2$ sublevels which lie above the ^{1}S ground state by 21 850.405, 21 870.464, and 21 911.178 cm^{-1}, respectively.[52] Since the $B'\,^2\Sigma^+$ state potential curve lies below that of the $A\,^2\Pi$ state at large internuclear distances (Fig. 3), we conclude that the $B'\,^2\Sigma^+$ ($\Omega = 1/2$) and the $A\,^2\Pi$ ($\Omega = 1/2, 3/2$) states dissociate into $^3P_0$, and $^3P_1$ sublevels, respectively. Using the T_0 values listed in Table IV, the D_0 dissociation energies for the $A\,^2\Pi$ and $B'\,^2\Sigma^+$ states were found to be 12 957.5 ± 0.5 and 10 133.6 ± 0.5 cm^{-1}, respectively, and the corresponding D_e values are 13 749.6 ± 0.5 and 10 545.0 ± 0.5 cm^{-1}, respectively.

E. Determination of electronic matrix elements (a^+ and b)

The RKR potential curves (turning points) listed in Tables VII and S8 were used in Le Roy's program LEVEL,[53] and the vibrational integrals $\langle v_\Pi \mid v_\Sigma \rangle$ and B_{v_Π, v_Σ} connecting the $A\,^2\Pi$ and $B'\,^2\Sigma^+$ states were calculated. These matrix elements depend rather strongly on the rotational quantum number N of the $^2\Sigma^+$ state. For each pair of interacting vibrational levels, the matrix elements at a specific N (at which the levels cross) are listed in Table VII. The signs of the above vibrational integrals depend on the phase choices used for the vibrational wavefunctions. A common convention, used in the program LEVEL, is that the vibrational wavefunctions with even or odd quantum numbers have opposite signs at the inner turning point. However, in the "universal" phase convention recommended by Lefebvre-Brion and Field,[54] all vibrational wavefunctions are positive at the inner turning point. We used the universal phase convention and multiplied all vibrational integrals from LEVEL by the factor $(-1)^{v_\Pi + v_\Sigma}$. The wavefunctions for $v_\Pi = 2$, $v_\Pi = 3$, and $v_\Sigma = 3$ are plotted in Fig. 4, and the numerical values of vibrational integrals $\langle v_\Pi \mid v_\Sigma \rangle$ and B_{v_Π, v_Σ} are presented in Table VII. Having the empirical a_{v_Π, v_Σ} and bB_{v_Π, v_Σ} constants from Table III,

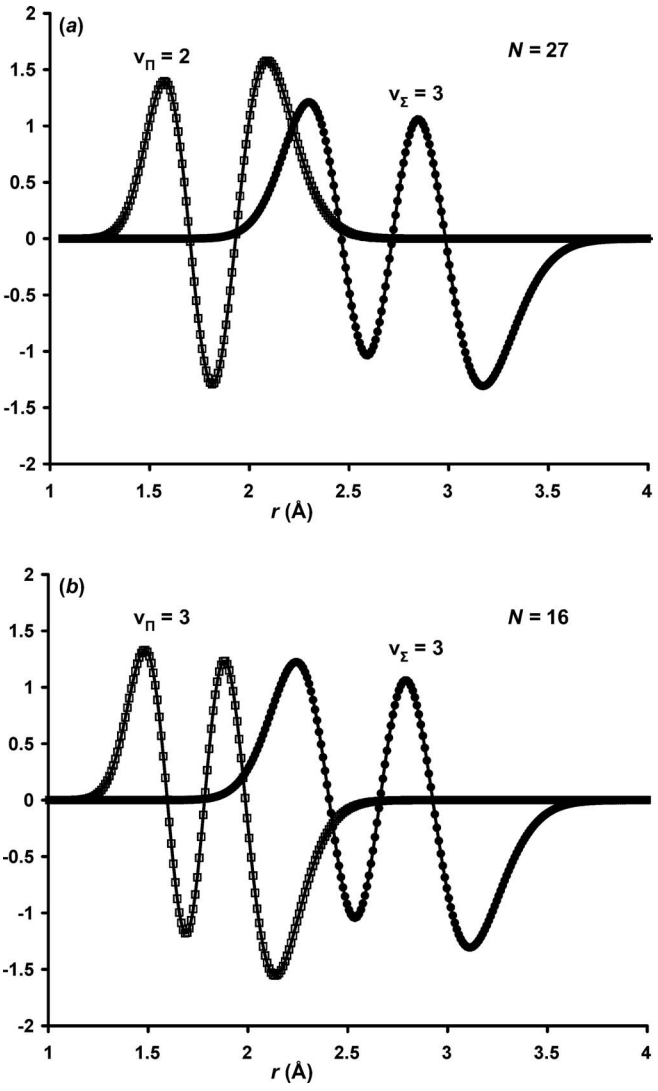

FIG. 4. (a) The $v_\Pi = 2$ and $v_\Sigma = 3$ vibrational wavefunctions at $N = 27$ generated by program LEVEL, showing a positive overlap integral. (b) The $v_\Pi = 3$ and $v_\Sigma = 3$ vibrational wavefunctions at $N = 16$, showing a negative overlap integral. The universal phase convention recommended by Lefebvre-Brion and Field (see Ref. 54) was used.

the purely electronic matrix elements $a^+ = \langle \pi | \, a l^+ \, | \sigma \rangle$ and $b = \langle \pi | \, l^+ \, | \sigma \rangle$ can be calculated from Eqs. (4) and (5). The numerical values of a^+ and b were determined for each (v_Π, v_Σ) pair independently (Table VII), and were averaged to give $a^+ = 19.0 \pm 0.3$ cm^{-1} and $b = 0.698 \pm 0.005$. Although it is clear from our deperturbation analysis that a^+ and b have the same sign, their absolute sign (+/–) cannot be determined from spectroscopic data.

IV. CONCLUSIONS

Term values for the v = 0 to 3 levels of the $A\,^2\Pi$ state and the v = 0 to 4 levels of the $B'\,^2\Sigma^+$ state of MgH were fitted together using a 15 × 15 Hamiltonian matrix, and deperturbed molecular constants were determined. A Dunham-type fit was performed and the resulting $Y_{l,0}$ and $Y_{l,1}$ coefficients were used to generate RKR potential curves for these states. Off-diagonal matrix elements $\langle v_\Pi \mid v_\Sigma \rangle$ and B_{v_Π, v_Σ} were computed from the RKR potentials, and the purely electronic a^+ and b matrix elements were determined. Using the accurate dissociation energy for the $X\,^2\Sigma^+$ ground state,[44] i.e., D_0 ($X\,^2\Sigma^+$) = 10 365.6 ± 0.5 cm^{-1}, the dissociation energies (D_0) of the $A\,^2\Pi$ and $B'\,^2\Sigma^+$ states were determined to be 12 957.5 ± 0.5 and 10 133.6 ± 0.5 cm^{-1}, respectively. The equilibrium internuclear distances (r_e) of the $A\,^2\Pi$ and $B'\,^2\Sigma^+$ states are 1.67827(1) Å and 2.59404(4) Å, respectively.

ACKNOWLEDGMENTS

We thank the Leverhulme Trust for some financial support to P.F.B. through a Research Project Grant. The spectra of MgH were recorded at the University of Waterloo.

[1] A. Fowler, Mon. Not. R. Astron. Soc. **67**, 530 (1907).
[2] A. Fowler, Philos. Trans. R. Soc. London, Ser. A **209**, 447 (1909).
[3] P. Sotirovski, Astron. Astrophys. Suppl. Ser. **6**, 85 (1972); http://adsabs.harvard.edu/cgi-bin/nph-bib_query?1972A%26AS....6...85S&db_key=AST.
[4] L. Wallace, K. Hinkle, G. Li, and P. F. Bernath, Astrophys. J. **524**, 454 (1999).
[5] J. D. Kirkpatrick, Annu. Rev. Astron. Astrophys. **43**, 195 (2005).
[6] A. M. Boesgaard, Astrophys. J. **154**, 185 (1968).
[7] P. L. Gay and D. L. Lambert, Astrophys. J. **533**, 260 (2000).
[8] W. W. Watson and P. Rudnick, Astrophys. J. **63**, 20 (1926).
[9] W. W. Watson and P. Rudnick, Phys. Rev. **29**, 413 (1927).
[10] R. S. Mulliken, Phys. Rev. **32**, 388 (1928).
[11] R. W. B. Pearse, Proc. R. Soc. A **122**, 442 (1928).
[12] Y. Fujioka and Y. Tanaka, Sci. Pap. Inst. Phys. Chem. Res. (Jpn.) **30**, 121 (1936).
[13] B. Grundström, Nature (London) **137**, 108 (1936).
[14] A. Guntsch, Z. Phys. **104**, 584 (1937).
[15] L. A. Turner and W. T. Harris, Phys. Rev. **52**, 626 (1937).
[16] A. Guntsch, Z. Phys. **107**, 420 (1937).
[17] K. P. Huber and G. Herzberg, *Molecular Spectra and Molecular Structure IV. Constants of Diatomic Molecules* (Van Nostrand, New York, 1979).
[18] W. J. Balfour, Astrophys. J. **162**, 1031 (1970).
[19] W. J. Balfour, J. Phys. B **3**, 1749 (1970).
[20] W. J. Balfour and H. M. Cartwright, Chem. Phys. Lett. **32**, 82 (1975).
[21] W. J. Balfour and H. M. Cartwright, Can. J. Phys. **53**, 1477 (1975).
[22] W. J. Balfour and H. M. Cartwright, Can. J. Phys. **54**, 1898 (1976).
[23] W. J. Balfour and H. M. Cartwright, Astron. Astrophys. Suppl. Ser. **26**, 389 (1976); http://adsabs.harvard.edu/cgi-bin/nph-bib_query?1976A%26AS...26..389B&db_key=AST.
[24] W. J. Balfour and B. Lindgren, Can. J. Phys. **56**, 767 (1978).
[25] W. J. Balfour, J. Mol. Spectrosc. **79**, 507 (1980).
[26] P. F. Bernath, J. H. Black, and J. W. Brault, Astrophys. J. **298**, 375 (1985).
[27] B. Lemoine, C. Demuynck, J. L. Destombes, and P. B. Davies, J. Chem. Phys. **89**, 673 (1988).
[28] K. R. Leopold, L. R. Zink, K. M. Evenson, D. A. Jennings, and M. Mizushima, J. Chem. Phys. **84**, 1935 (1986).
[29] L. R. Zink, Ph.D. dissertation, University of Colorado, 1986.
[30] L. R. Zink, D. A. Jennings, K. M. Evenson, and K. R. Leopold, Astrophys. J. **359**, L65 (1990).
[31] L. M. Ziurys, W. L. Barclay, Jr., and M. A. Anderson, Astrophys. J. **402**, L21 (1993).
[32] A. Shayesteh, D. R. T. Appadoo, I. Gordon, R. J. Le Roy, and P. F. Bernath, J. Chem. Phys. **120**, 10002 (2004).
[33] W. Meyer and P. Rosmus, J. Chem. Phys. **63**, 2356 (1975).
[34] M. L. Sink, A. D. Bandrauk, W. H. Henneker, H. Lefebvre-Brion, and G. Raseev, Chem. Phys. Lett. **39**, 505 (1976).
[35] R. P. Saxon, K. Kirby, and B. Liu, J. Chem. Phys. **69**, 5301 (1978).
[36] K. Kirby, R. P. Saxon, and B. Liu, Astrophys. J. **231**, 637 (1979).
[37] M. L. Sink and A. D. Bandrauk, Can. J. Phys. **57**, 1178 (1979).
[38] P. F. Weck, A. Schweitzer, P. C. Stancil, P. H. Hauschildt, and K. Kirby, Astrophys. J. **582**, 1059 (2003).
[39] P. F. Weck, P. C. Stancil, and K. Kirby, Astrophys. J. **582**, 1263 (2003).
[40] P. F. Weck, A. Schweitzer, P. C. Stancil, P. H. Hauschildt, and K. Kirby, Astrophys. J. **584**, 459 (2003).
[41] S. Skory, P. F. Weck, P. C. Stancil, and K. Kirby, Astrophys. J., Suppl. Ser. **148**, 599 (2003).
[42] J.-M. Mestdagh, P. de Pujo, B. Soep, and F. Spiegelman, Chem. Phys. Lett. **471**, 22 (2009).
[43] M. Guitou, A. Spielfiedel, and N. Feautrier, Chem. Phys. Lett. **488**, 145 (2010).
[44] A. Shayesteh, R. D. E. Henderson, R. J. Le Roy, and P. F. Bernath, J. Phys. Chem. A **111**, 12495 (2007).
[45] See supplementary material at http://dx.doi.org/10.1063/1.3631341 for a complete list of data and constants.
[46] J. M. Brown, E. A. Colbourn, J. K. G. Watson, and F. D. Wayne, J. Mol. Spectrosc. **74**, 294 (1979).
[47] P. F. Bernath, *Spectra of Atoms and Molecules*, 2nd ed. (Oxford University Press, New York, 2005).
[48] H. Lefebvre-Brion and R. W. Field, *The Spectra and Dynamics of Diatomic Molecules* (Elsevier/Academic, Amsterdam, 2004).
[49] L. A. Kaledin, J. C. Bloch, M. C. McCarthy, and R. W. Field, J. Mol. Spectrosc. **197**, 289 (1999).
[50] R. J. Le Roy, RKR1 2.0, University of Waterloo Chemical Physics Research Report CP-657R, 2004; see http://leroy.uwaterloo.ca.
[51] R. J. Le Roy, DPARFIT 3.3, University of Waterloo Chemical Physics Research Report CP-660, 2005; see http://leroy.uwaterloo.ca.
[52] See http://physics.nist.gov/PhysRefData/Handbook/element_name.htm for NIST Basic Atomic Spectroscopic Data.
[53] R. J. Le Roy, LEVEL 8.0, University of Waterloo Chemical Physics Research Report CP-663, 2007; see http://leroy.uwaterloo.ca.
[54] H. Lefebvre-Brion and R. W. Field, *The Spectra and Dynamics of Diatomic Molecules* (Elsevier/Academic, Amsterdam, 2004), p. 291.